On-Surface Synthesis

International Edition: DOI: 10.1002/anie.201900636
German Edition: DOI: 10.1002/ange.201900636

Surface-Dependent Chemoselectivity in C–C Coupling Reactions

Zhi Chen, Tao Lin,* Liding Zhang, Lei Zhang, Bingxi Xiang, Hu Xu, Florian Klappenberger,* Johannes V. Barth, Svetlana Klyatskaya, and Mario Ruben**

Abstract: *Surface-confined covalent coupling reactions of the linear compound 4-(but-3-en-1-ynyl)-4′-ethynyl-1,1′-biphenyl (**1**), which contains one alkyne and one enyne group on opposing ends, have been investigated using scanning tunneling microscopy (STM) and density functional theory (DFT) calculations. The reactions show a surface-dependent chemoselectivity: on Au(111), compound **1** preferentially yields cyclotrimerization products, while on Cu(111), a selective coupling between the enyne and alkyne groups is observed. Linear, V-shaped string formations combined with Y-shaped bifurcation motifs result in a random reticulation on the entire surface. DFT calculations show that the C–H$\cdots\pi^{\delta-}$ transition state of the reaction between the deprotonated alkyne group and a nearby H-donor of the alkene group plays a key role in the mechanism and high chemoselectivity. This study highlights a concept that opens new avenues to the surface-confined synthesis of covalent carbon-based sp–sp^2 polymers.*

In the past decade, on-surface reactions have been shown to enable the detailed investigation of reaction mechanisms, since some stable intermediates can be directly observed at the sub-molecular level by scanning probe microscopy. Moreover, on-surface reactions also provide an innovative route for the bottom-up fabrication of one-dimensional (1D) wires or ribbons, and two-dimensional (2D) covalent organic frameworks including certain graphene analogues, which show significant potential for applications in molecular electronics and optoelectronics.[1] Notable reactions such as Ullmann coupling and Glaser coupling have been widely investigated on surfaces.[1b]

Due to their increased reactivity, alkyne compounds have been used in a multitude of on-surface studies.[2] Reactions such as azide–alkyne cycloaddition,[3] cyclotrimerization,[4] and homo-coupling[5] have been investigated on Cu(111),[5b,6] Au(111),[4,5d,e] and Ag(111),[5a,c,e,f] and a preference for cyclotrimerization and homo-coupling was observed on Au(111)[4] and Ag(111),[5a,c] respectively. However, on Cu(111), a variety of reactions is observed[5b] and even organometallic alkyne complexes can evolve during annealing.[5c,d,7] Due to the high reactivity, achieving the C–C homo-coupling of alkynes with a low number of side reactions on Cu(111) remains a challenge.

Compared with terminal alkynes, terminal alkene compounds show a lower reactivity in general, which is attributed to the lower σ-character and electronegativity of their carbon atoms, that is, terminal alkenes normally do not react on Au(111) and Cu(111) surfaces. However, it was shown that on Cu(110), they can be coupled into (*Z*,*Z*)-butadiene with high stereoselectivity.[8]

Until now, studies of on-surface chemical reactions have been mainly focusing on homo-coupling reactions. On-surface cross-coupling reactions are mostly observed between aromatic halogen compounds and alkynes, and the activation of additional precursors would enlarge the scope of this reaction type.[9] In solution, such cross-coupling reactions have been proven to be more challenging, since alkyne and alkene groups prefer to undergo enyne metathesis reactions[10] or addition reactions.[11] Only a single example has been reported in which electron-deficient olefins and alkynes could be coupled by a Pd catalyst, yielding the desired cross-coupling enyne products.[12] Under surface confinement, the cross-coupling of alkynes (with sp carbon atoms) and alkenes (with sp^2 carbon atoms) has not been studied yet.

With this aim in mind, we designed and synthesized the compound 4-(but-3-en-1-ynyl)-4′-ethynyl-1,1′-biphenyl (**1**; Scheme 1), which contains one alkyne and one enyne substituent on a biphenyl backbone and acts as a precursor in on-surface reactions. These functional groups may lead to the formation of several symmetric products based on homo-coupling reactions along with cross-coupling, leading to a set of regioisomers. Using compound **1**, we performed systematic investigations on well-defined Au(111) and Cu(111) substrates by scanning tunneling microscopy (STM). The analysis was supported by DFT simulations. For the first time, a very effective coupling between alkyne and enyne groups under

[*] Dr. Z. Chen, Dr. S. Klyatskaya, Prof. Dr. M. Ruben
Institute of Nanotechnology, Karlsruhe Institute of Technology (KIT)
76344 Eggenstein-Leopoldshafen (Germany)
E-mail: zhi.chen@partner.kit.edu
mario.ruben@kit.edu
Dr. T. Lin, L. Zhang, Dr. F. Klappenberger, Prof. Dr. J. V. Barth
Department of Physics E20, Technical University of Munich (TUM)
85748 Garching (Germany)
E-mail: florian.klappenberger@tum.de
lintao@sztu.edu.cn
Dr. L. Zhang, Prof. Dr. H. Xu
Department of Physics, Southern University of Science and Technology, Shenzhen 518055 (China)
Prof. Dr. M. Ruben
IPCMS-CNRS, Université de Strasbourg
Strasbourg F-67034 (France)
Dr. Z. Chen
International Collaborative Laboratory of 2D Materials for Optoelectronics Science and Technology of Ministry of Education, College of Physics and Optoelectronic Engineering, Shenzhen University
Shenzhen 518060 (China)
Dr. T. Lin, Dr. B. Xiang
College of New Materials and New Energies, Shenzhen Technology University, Shenzhen 518118 (China)
E-mail: lintao@sztu.edu.cn
Supporting information and the ORCID identification number(s) for the author(s) of this article can be found under: https://doi.org/10.1002/anie.201900636.

 © 2019 Wiley-VCH Verlag GmbH & Co. KGaA, Weinheim

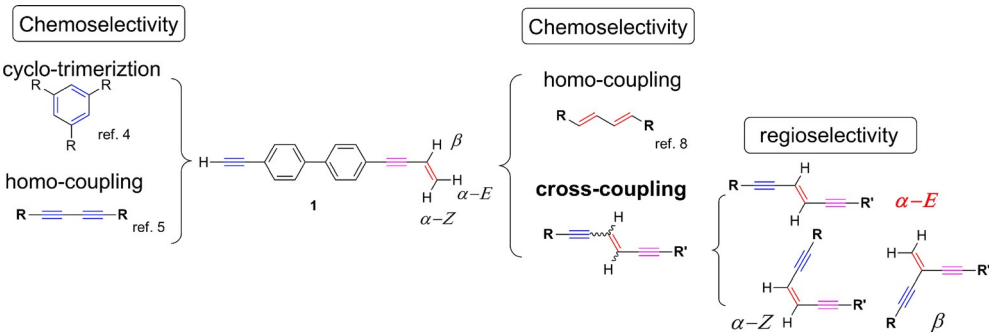

Scheme 1. Possible transformation pathways of compound **1**.

on-surface conditions is reported and further developed into large-scale 2D covalent networks.

The molecular structure of the custom-designed compound **1** is depicted in the Scheme 1. **1** can be described as an asymmetrical molecule with one 1,3-enyne group in the 4 position and an alkyne group in the 4′ position of a biphenyl backbone. In the alkene group, there are three reactive hydrogen atoms, labeled α-*E*, α-*Z*, and *β* (see Scheme 1).

First, a 0.3-monolayer (ML) coverage of **1** was deposited onto the Au(111) substrate, which was held at 273 K. An individual molecule of **1** appears as a rod-like protrusion with a bright lobe at one end (Figure 1 a). The bright lobe can be ascribed to the enyne group (marked by the red arrows in Figure 1 b). Aside from individual molecules, self-assembled aggregates with windmill-, triangle-, and square-like shapes are also observed. Upon deposition, the molecules preferentially occupy elbow sites of the herringbone reconstruction of the Au(111) substrate. After increasing the coverage to 0.8 ML, compound **1** begins to grow along the fcc stripes in an irregular manner (Figure 1 c).

Three different types of supramolecular interactions drive the formation of the self-assembled aggregates: i) weak intermolecular C–H···π interactions between the hydrogen atom of the terminal alkyne group and the π-system of the enyne group of a nearby molecule **1**, which can be observed as triangle-like patterns (red circles in Figure 1 a, c, see also Figure 1 b-i; statistical value: 2 %) and rhombus-like aggregates (yellow circles in Figure 1 a, c, see also Figure 1 b-ii; 1 %). ii) Intermolecular C–H···π interactions between the hydrogen atom of the terminal alkyne group and the π-system of the terminal alkyne group of a neighboring molecule **1**, observed as fourfold-symmetrical windmill-shaped nodes (green circles in Figure 1 a, c, see also Figure 1 b-iii; 80 %)[4b,9a] as well as five-fold (blue circles in Figure 1 c, see also Figure 1 b-iv; 7 %) and six-fold windmill-shaped nodes (purple circles in Figure 1 c, see also Figure 1 b-v; 5 %).[4b,13] Additionally, there are irregular monomers and dimer nodes, which occupy the residual statistical value of 5 %. iii) Weak C–H···π interactions between two enyne groups of nearby molecules **1**; observed in regular close-packed reticular fourfold-symmetrical assemblies (Figure S3, Supporting Information). Each supramolecular node (threefold- to sixfold-symmetrical nodes) exhibits chirality as either an *R* or *S* enantiomer (solid circles and dashed circles for *R* and *S*, respectively, in Figure 1).[14] When carefully analyzing the enantiomorphic distribution within these regular domains, we find that it represents a 2D racemic crystal with line-type stacking phases (Figure S3 b),[14d,15] closest-neighbor phases (Figure S3 c),[14a,c,d] and mixed phases (Figure S3 d).[14d]

After annealing the sample at 393 K for 10 min, the majority of the molecules **1** undergo cyclotrimerization (Figure 1 e-i, blue circles in Figure 1 d; 45 %, see also Figure S4) resulting in molecular islands on the surface. There is a bright lobe at each end of the Y-shaped cyclotrimerization products (red arrows in Figure 1 e-i), indicating that the cyclotrimerization occurs between the alkyne groups. Moreover, some tetramers (Figure 1 e-ii, green circles in Figure 1 d; 5 %) also exist due to the reaction between an enyne group of the cyclotrimerization product with an alkyne group of another molecule **1**, but they cannot extend to 1D or 2D structures. It should be noted that, additionally, a small amount of dimers (Figure 1 e-iii, orange arrows in Figure 1 d; 10 %) is present on the surface. There are also some unreacted monomers and possibly organometallic intermediates, which are accounted for under "other" (purple arrows in Figure 1 d).

To trigger further oligomerization of the remaining pristine molecules, we annealed the sample to 433 K for 10 min. As shown in Figures 1 f and S5, the molecular coverage decreases, indicating that some molecules desorb from the substrate, but further reactions hardly occur during annealing.

Due to the lowered activity of the enyne group on Au(111), we changed the substrate to Cu(111). As a first approach, a 0.3 ML coverage of molecules **1** was deposited onto the Cu(111) substrate, which was held at ≈200 K. As shown in Figure 2 a, molecules of **1** are scattered over the surface and the majority remains isolated. Their appearance, a rod-like protrusion with a bright lobe at one end, reflects the situation observed on Au(111). Accordingly, the bright-lobe feature is again attributed to the enyne group (red arrows in Figure S6). The molecule–substrate interaction reveals a preferential molecular arrangement along the $<11\bar{2}>$ set of directions. Additionally, guided by weak intermolecular interactions, some molecules form short supramolecular linear aggregates (Figure S6), which can be considered as a suitable predisposition for the C–C coupling reaction. The DFT-optimized adsorption geometry (Figure 3 a, b) and simulated STM images (calculated at a bias voltage of −1 V;

 © 2019 Wiley-VCH Verlag GmbH & Co. KGaA, Weinheim

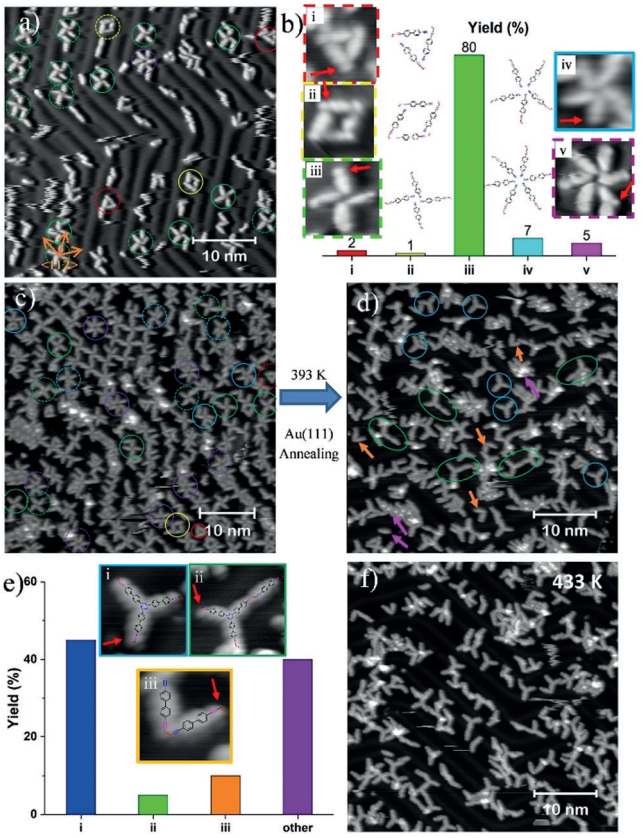

Figure 1. a) Initial deposition of **1** on Au(111) held at 273 K with ca. 0.3 ML coverage. The orange arrows show the $<11\bar{2}>$ set of directions of Au(111). b) Close-up STM images of five kinds of isolated supramolecular nodes (i–v) upon self-assembly of **1** on Au(111), and the statistical results of different self-assembly nodes based on (c). Chemical models of the different nodes are also shown. Red arrows show the bright lobe attributed to the enyne groups. c) STM image of the self-assembly upon deposition of **1** on Au(111) held at 273 K with ca. 0.8 ML coverage. Circles with different colors show different kinds of supramolecular nodes. Solid and dashed circles indicate a chiral geometry with *R* or *S* enantiomorphs, respectively. d) STM image of products of **1** on Au(111) after thermal annealing at 393 K. Different colors show different annealing products. e) Close-up STM images of three types of isolated annealing products (i–iii). Each image of (e) is superposed with a tentative chemical model and red arrows pointing towards the bright lobes ascribed to the enyne groups. The bottom panel presents the statistical results of different annealing products: i) cyclotrimerization, ii) tetramerization, iii) dimerization, and other. f) STM image of the annealing products of **1** on Au(111) after thermal treatment at 433 K. Scanning parameters for (a–f): $U_{bias} = -1$ V, $I_t = 0.1$ nA.

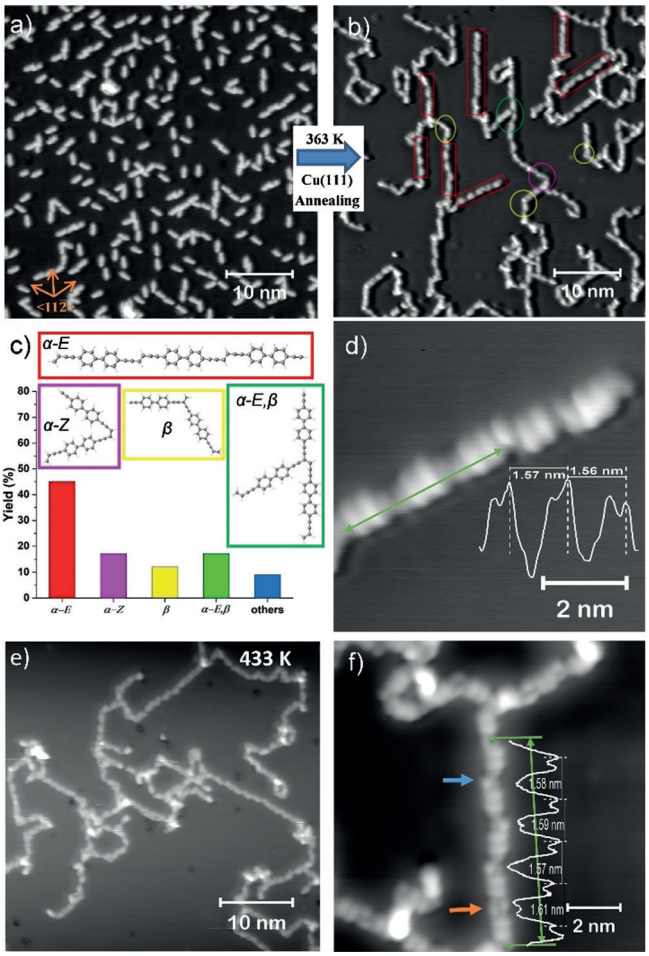

Figure 2. a) STM image of deposited molecules **1** (0.3 ML) on Cu(111) at a substrate temperature of 200 K. Orange arrows show the $<11\bar{2}>$ set of directions of Cu(111). b) Polymerization of **1** on Cu(111) after annealing at 363 K. Colors relate to distinct oligomer types of the covalent 2D network. c) Four types of covalent linkages present in chain segments shown in (b) together with a graph depicting the relative abundance of the coupling motifs according to the statistical evaluation. d) Zoomed-in STM image of a 1D chain polymer of **1** from (b). Inset: Line-scan profile of the polymer marked by the green line. e), f) Polymerization of **1** on Cu(111) after annealing at 433 K. The blue and orange arrows in (f) highlight single- and double-Cu-coordinated sites, respectively. Inset of (f): Line-scan profile of the polymer between the two green spots. Scanning parameters: (a) $U_{bias} = -0.9$ V, $I_t = 0.1$ nA; (b, d, e, f): $U_{bias} = -1$ V, $I_t = 0.1$ nA.

Figure 3c,d) of compound **1** on Cu(111) show that the terminal alkyne group appears slightly dark whereas the enyne group appears as a bright lobe, which is in good agreement with the experimental results (Figure S6). This suggests that the alkyne groups form a coordinative bond to the Cu(111) surface at 200 K, which is in good agreement with reports about terminal alkyne adsorption on Cu(111) in the literature.[6,16]

After annealing at 333 K for 10 min, short 1D linear chain segments become visible on Cu(111), indicating that this thermal treatment triggers the formation of covalent C–C bonds (Figure S7). By further annealing at 363 K, the 1D linear chain segments grow longer. In contrast to the dominating cyclotrimerization of **1** on Au(111), the main reaction on the Cu(111) substrate is the cross-coupling reaction of the enyne and alkyne groups between two molecules **1**. The presence of three reactive hydrogen sites on the alkene moiety enables several chain motifs via formation of three different cross-coupling products: i) at α-*E* (red rectangles in Figure 2b, 2c-α-*E*; 45%), ii) at α-*Z* (purple circles in Figure 2b, 2c-α-*Z*; 17%), and at the *β*-hydrogen (yellow circles in Figure 2b, 2c-*β*; 12%). Interestingly, the latter two exhibit V-shape configurations with

 © 2019 Wiley-VCH Verlag GmbH & Co. KGaA, Weinheim

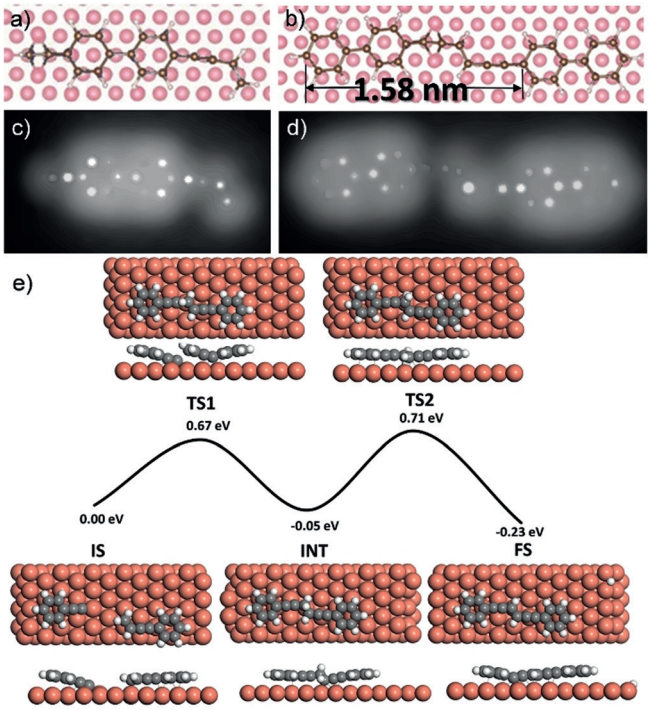

Figure 3. a), b) Energetically favored adsorption geometry of **1** (a) and the molecular dimer (b) on Cu(111), obtained from DFT calculations. c), d) Simulated STM images ($U = -1$ V) of **1** (c) and the molecular dimer (d). Color code: Cu, orange; C, gray; H, white. e) DFT-calculated reaction path for the cross-coupling reaction of the terminal alkyne with the enyne, shown in side and top views of the initial state (IS), the transition states (TS1 and TS2), the intermediate state (INT), and the final state (FS). The respective phenyl derivatives of **1** were used.

angles of 60° and 120°, respectively. When the cross-coupling occurred simultaneously at two reactive hydrogen sites (for example, α-*E*,*β*), branched Y-shape-like connection nodes (green circles in Figure 2b, 2c-α-*E*,*β*; 17%) are observed. These nodes link nearby oligomeric strands and represent the elementary motif of the resulting disordered 2D covalent network. Furthermore, the majority of the 1D wires are arranged along the $<11\bar{2}>$ set of directions. To further verify the reaction products, we measured the distance of the repeating unit (Figure 2d), yielding a value of 1.57 ± 0.06 nm, which is in good agreement with the distance of 1.58 nm for a model obtained by DFT calculations (Figure 3b). Similar to absorbed monomer molecules **1**, the optimized model (Figure 3b) and simulated STM image (Figure 3d) of the elementary cross-coupling product are in good agreement with the experimental data shown in Figure 2d. Interestingly, the central part the of the akynyl–alkenyl–alkynyl bridge exhibits a slightly darker feature on Cu(111) (Figures 2d and 3d).

To trigger further oligomerization, the sample was annealed to 433 K (Figures 2e,f and S8). The obtained structure now displays a 2D covalent network dominatingly consisting of linear C–C-linkages and Y-shaped interconnections resulting from single and double cross-coupling products, thus representing an efficient way for the on-surface construction of mixed sp–sp^2 carbon scaffolds. We find that often, there are one or two bright spots along each alkyne–alkene linkage in the sample annealed at 433 K (marked by the blue and orange arrows in Figure 2f and the orange arrow in Figure S10b, top-right inset). Measurements of the repeating-unit distance show that the units are in a perfect distance of 1.59 ± 0.06 nm of each other (Figure 2f), which is almost the same as observed in the sample annealed at 363 K (Figure 2d). We assume that Cu atoms are pulled out of the substrate and coordinate side-on to the alkyne–alkene–alkyne linker of the polymer. One bright spot can be attributed to the changed geometry of the fragment, which is also supported by the DFT-calculated structure and STM image (Figures 3d and S9).

First-principle calculations were performed to gain further insight into the mechanistic aspects of the alkyne–enyne cross-coupling on Cu(111). Figure 3a–d displays the most favorable adsorption geometries of the monomer **1** and the product of the alkyne–enyne cross-coupling along with simulated STM images. The molecular orientations are perfectly compatible with those observed in experiment. To simplify the modeling, we applied phenylacetylene and 3-buten-1-yn-1-yl-benzene as the cross-coupling reagents. Theoretical calculations reveal that the dehydrogenation process of the terminal alkynes on Cu(111) is catalyzed by a Cu-adatom, followed by the formation of organometallic intermediates,[6,16] as evidenced by the characteristic terminal depressions at the terminal alkyne groups. Similar effects were observed upon annealing to 333 K (Figure S7). Thus, we directly used the phenylacetylide in the simulation of the initial state (Figure 3e, IS). The attraction of the alkyne group at the enyne end in reagent 3-buten-1-yn-1-yl-benzene towards the Cu(111) surface lifts the alkene groups relatively far from the substrate (Figure 3e, TS1). Here, the deprotonated alkyne group forms an ionic C–H$\cdots\pi^{\delta-}$ hydrogen bond between the π-system of the deprotanted alkynyl group and a nearby H-donor,[6] resulting in a coupling transition state.[17] The DFT results shown in Figure 3e (TS1) confirm that the hydrogen atom of the alkene group acts as a very good H-donor in the formation of the ionic C–H$\cdots\pi^{\delta-}$ hydrogen bond. This enables the formation of a cross-coupling intermediate state (Figure 3e, INT), followed by direct dehydrogenation with an energy barrier of 0.76 eV (Figure 3e, TS2 and FS). In contrast, the Au(111) surface is inactive towards deprotonation of the terminal alkyne as well as alkene-group activation at the given temperature,[8] resulting exclusively in cyclotrimerization instead of C–H bond dissociations.[4]

The effect of the coverage on the outcome of the cross-coupling reaction was investigated for 0.8 ML of **1** on Cu(111) (Figure S10a). The resulting supramolecular organization is not very regular, which is attributed to the strong interaction of the alkyne and enyne groups with the Cu(111) surface, inhibiting a thermodynamic self-assembly. Upon annealing at 433 K, a covalent network has formed through selective cross-coupling reactions (Figures S10b and S11), which decorates the entire surface in a branched fashion. Upon increasing the surface coverage, the formation of long straight 1D chains with favorable α-*E*-site cross-coupling (Figure 2b) is slowly declining; at increased coverages, the α-*Z*- and *β*-site cross-couplings are becoming more prominent, leading to V- and Y-

 © 2019 Wiley-VCH Verlag GmbH & Co. KGaA, Weinheim

shaped branching nodes and a shortening of the 1D wire segments, which finally leads to a network with irregular pores.

In conclusion, C–C coupling reactions of the ditopic compound **1** have been investigated on Au(111) and Cu(111) using STM and DFT. On Au(111), **1** mainly forms cyclotrimerization products related to the terminal alkyne functionalization. On the Cu(111) surface, enyne groups can chemoselectively cross-couple with alkyne groups, affording 1D wires that are further branched to 2D covalent networks. DFT calculations show that the C–H···$\pi^{\delta-}$ transition state of the reaction between the deprotonated alkyne group and a nearby alkene group is a key point for the chemoselective alkyne–alkene cross-coupling on Cu(111). This work reports the first alkyne–alkene cross-coupling reaction on metallic substrates, which opens a new route towards the on-surface fabrication of covalent polymers. Based on the gained insights, we expect, on the long term, the development of improved chemoselectivity of the cross-coupling reaction on surfaces to yield 1D molecular wires and ribbons or 2D networks useful for molecular electronic applications.[5f]

Acknowledgements

This work is supported by the DFG via KL 2294/6-1 and the priority program 1459, and the Excellence Cluster Munich-Centre for Advanced Photonics (MAP), the European Union via the FET project 2d-ink (grant agreement 664878), the National Natural Science Foundation of China (No. 21802067), the Shenzhen Science and Technology Planning (No. JCYJ20170818143327496) and the China Scholarship Council (Z.C.). L.Z. thanks the IMPRS-APS for support, T.L. thanks the TUM University Foundation for a postdoctoral fellowship.

Conflict of interest

The authors declare no conflict of interest.

Keywords: alkenes · alkynes · chemoselectivity · cross-coupling · scanning tunneling microscopy

How to cite: *Angew. Chem. Int. Ed.* **2019**, *58*, 8356–8361
Angew. Chem. **2019**, *131*, 8444–8449

[1] a) G. Franc, A. Gourdon, *Phys. Chem. Chem. Phys.* **2011**, *13*, 14283–14292; b) J. Björk, F. Hanke, *Chem. Eur. J.* **2014**, *20*, 928–934; c) L. Dong, P. N. Liu, N. Lin, *Acc. Chem. Res.* **2015**, *48*, 2765–2774; d) F. Klappenberger, Y. Q. Zhang, J. Björk, S. Klyatskaya, M. Ruben, J. V. Barth, *Acc. Chem. Res.* **2015**, *48*, 2140–2150; e) L. Talirz, P. Ruffieux, R. Fasel, *Adv. Mater.* **2016**, *28*, 6222–6231.

[2] G. N. Patwari, P. Venuvanalingam, M. Kołaski, *Chem. Phys.* **2013**, *415*, 150–155.

[3] a) O. Díaz Arado, H. Mönig, H. Wagner, J.-H. Franke, G. Langewisch, P. A. Held, A. Studer, H. Fuchs, *ACS Nano* **2013**, *7*, 8509–8515; b) F. Bebensee, C. Bombis, S.-R. Vadapoo, J. R. Cramer, F. Besenbacher, K. V. Gothelf, T. R. Linderoth, *J. Am. Chem. Soc.* **2013**, *135*, 2136–2139.

[4] a) J. Liu, P. Ruffieux, X. L. Feng, K. Müllen, R. Fasel, *Chem. Commun.* **2014**, *50*, 11200–11203; b) H. Zhou, J. Liu, S. Du, L. Zhang, G. Li, Y. Zhang, B. Z. Tang, H.-J. Gao, *J. Am. Chem. Soc.* **2014**, *136*, 5567–5570.

[5] a) Y.-Q. Zhang, N. Kepčija, M. Kleinschrodt, K. Diller, S. Fischer, A. C. Papageorgiou, F. Allegretti, J. Björk, S. Klyatskaya, F. Klappenberger, M. Ruben, J. V. Barth, *Nat. Commun.* **2012**, *3*, 1286; b) J. Eichhorn, W. M. Heckl, M. Lackinger, *Chem. Commun.* **2013**, *49*, 2900–2902; c) J. Liu, Q. Chen, L. Xiao, J. Shang, X. Zhou, Y. Zhang, Y. Wang, X. Shao, J. Li, W. Chen, G. Q. Xu, H. Tang, D. Zhao, K. Wu, *ACS Nano* **2015**, *9*, 6305–6314; d) Q. Sun, L. Cai, H. Ma, C. Yuan, W. Xu, *ACS Nano* **2016**, *10*, 7023–7030; e) H. Y. Gao, H. Wagner, D. Zhong, J. H. Franke, A. Studer, H. Fuchs, *Angew. Chem. Int. Ed.* **2013**, *52*, 4024–4028; *Angew. Chem.* **2013**, *125*, 4116–4120; f) B. Cirera, Y. Q. Zhang, J. Björk, S. Klyatskaya, Z. Chen, M. Ruben, J. V. Barth, F. Klappenberger, *Nano Lett.* **2014**, *14*, 1891–1897.

[6] Y.-Q. Zhang, J. Björk, P. Weber, R. Hellwig, K. Diller, A. C. Papageorgiou, S. C. Oh, S. Fischer, F. Allegretti, S. Klyatskaya, M. Ruben, J. V. Barth, F. Klappenberger, *J. Phys. Chem. C* **2015**, *119*, 9669–9679.

[7] P. B. Weber, R. Hellwig, T. Paintner, M. Lattelais, M. Paszkiewicz, P. Casado Aguilar, P. S. Deimel, Y. Guo, Y. Q. Zhang, F. Allegretti, A. C. Papageorgiou, J. Reichert, S. Klyatskaya, M. Ruben, J. V. Barth, M. L. Bocquet, F. Klappenberger, *Angew. Chem. Int. Ed.* **2016**, *55*, 5754–5759; *Angew. Chem.* **2016**, *128*, 5848–5853.

[8] Q. Sun, L. Cai, Y. Ding, L. Xie, C. Zhang, Q. Tan, W. Xu, *Angew. Chem. Int. Ed.* **2015**, *54*, 4549–4552; *Angew. Chem.* **2015**, *127*, 4632–4635.

[9] a) T. Wang, H. Lv, Q. Fan, L. Feng, X. Wu, J. Zhu, *Angew. Chem. Int. Ed.* **2017**, *56*, 4762–4766; *Angew. Chem.* **2017**, *129*, 4840–4844; b) C. Sanchez-Sanchez, N. Orozco, J. P. Holgado, S. K. Beaumont, G. Kyriakou, D. J. Watson, A. R. Gonzalez-Elipe, L. Feria, J. Fernández Sanz, R. M. Lambert, *J. Am. Chem. Soc.* **2015**, *137*, 940–947; c) R. Zhang, G. Lyu, D. Y. Li, P. N. Liu, N. Lin, *Chem. Commun.* **2017**, *53*, 1731–1734; d) T. Wang, J. Huang, H. Lv, Q. Fan, L. Feng, Z. Tao, H. Ju, X. Wu, S. L. Tait, J. Zhu, *J. Am. Chem. Soc.* **2018**, *140*, 13421–13428; e) K. J. Shi, C. H. Shu, C. X. Wang, X. Y. Wu, H. Tian, P. N. Liu, *Org. Lett.* **2017**, *19*, 2801–2804.

[10] S. T. Diver, A. J. Giessert, *Chem. Rev.* **2004**, *104*, 1317–1382.

[11] a) K. Cheng, B. Yao, J. Zhao, Y. Zhang, *Org. Lett.* **2008**, *10*, 5309–5312; b) K. Kohno, K. Nakagawa, T. Yahagi, J. C. Choi, H. Yasuda, T. Sakakura, *J. Am. Chem. Soc.* **2009**, *131*, 2784–2785.

[12] V. Hadi, K. S. Yoo, M. Jeong, K. W. Jung, *Tetrahedron Lett.* **2009**, *50*, 2370–2373.

[13] N. Kepčija, Y.-Q. Zhang, M. Kleinschrodt, J. Björk, S. Klyatskaya, F. Klappenberger, M. Ruben, J. V. Barth, *J. Phys. Chem. C* **2013**, *117*, 3987–3995.

[14] a) F. Vidal, E. Delvigne, S. Stepanow, N. Lin, J. V. Barth, K. Kern, *J. Am. Chem. Soc.* **2005**, *127*, 10101–10106; b) M. Forster, M. S. Dyer, M. Persson, R. Raval, *Angew. Chem. Int. Ed.* **2010**, *49*, 2344–2348; *Angew. Chem.* **2010**, *122*, 2394–2398; c) N. Abdurakhmanova, A. Floris, T. C. Tseng, A. Comisso, S. Stepanow, A. De Vita, K. Kern, *Nat. Commun.* **2012**, *3*, 940; d) Y. Q. Zhang, T. Lin, B. Cirera, R. Hellwig, C. A. Palma, Z. Chen, M. Ruben, J. V. Barth, F. Klappenberger, *Angew. Chem. Int. Ed.* **2017**, *56*, 7797–7802; *Angew. Chem.* **2017**, *129*, 7905–7910.

[15] a) R. Cortes, A. Mascaraque, P. Schmidt-Weber, H. Dil, T. U. Kampen, K. Horn, *Nano Lett.* **2008**, *8*, 4162–4167; b) J. B. Lin, Z. X. Guo, J. Plas, D. B. Amabilino, S. De Feyter, A. P. H. J. Schenning, *Chem. Commun.* **2013**, *49*, 9320–9322; c) J. Seibel, M. Parschau, K.-H. Ernst, *J. Am. Chem. Soc.* **2015**, *137*, 7970–7973; d) M. Böhringer, W.-D. Schneider, R. Berndt, *Angew.*

 © 2019 Wiley-VCH Verlag GmbH & Co. KGaA, Weinheim

Chem. Int. Ed. **2000**, *39*, 792 – 795; *Angew. Chem.* **2000**, *112*, 821 – 825.
[16] T. Wang, H. Lv, L. Feng, Z. Tao, J. Huang, Q. Fan, X. Wu, J. Zhu, *J. Phys. Chem. C* **2018**, *122*, 14537 – 14545.
[17] J. Björk, Y.-Q. Zhang, F. Klappenberger, J. V. Barth, S. Stafström, *J. Phys. Chem. C* **2014**, *118*, 3181 – 3187.

Manuscript received: January 16, 2019
Revised manuscript received: April 5, 2019
Accepted manuscript online: April 24, 2019
Version of record online: May 14, 2019

 © 2019 Wiley-VCH Verlag GmbH & Co. KGaA, Weinheim